2023 IEEE/ASME International Conference on Advanced Intelligent Mechatronics (AIM)
June 28-30, 2023. Seattle, Washington, USA

Design and Control of 3-DOF Reluctance-force-type Magnetic Levitator Module for Fine-positioning Short-stroke Stage

Hyeong Min Yoon, Jae Woo Jung, Eun Kyu Kim, Jeong Min Park, Jong Min Sung, and Jun Young Yoon

Abstract— **This paper presents the design and control of a three degrees-of-freedom (3-DOF) magnetic levitation module for fine-positioning short-stroke actuators to be serially connected to high-acceleration long-stroke stages. The 3-DOF levitator module consists of two stator assemblies with iron-cores having actuating coils and permanent magnets (PMs) along the magnetic path. The levitating target is an U-shaped rotor with its weight passively compensated by the PM-biased flux and the lateral-direction force is balanced out by the symmetric structure. In such a magnetic levitator design, the PM-biased flux is superposed with the current-driven flux, enabling to control the reluctance forces in both the levitational and lateral directions in a decoupled manner to achieve active 3-DOF motion control. The control performance of the proposed 3-DOF magnetic levitator is experimentally validated to have RMS (root-mean-square) position tracking errors of 4.3 μm for the translation motions and 5.97 μdeg for the rotational motion. These control performances show a great potential of the magnetic levitation module to be utilized for fine-positioning short-stroke actuators that can overcome high inertial forces generated by serially-connected long-stroke actuators such as high-throughput linear stages and robotic arms.**

I. Introduction

Fine-positioning short-stroke stages are frequently used in various applications including the semiconductor [1], [2], [3] and flat panel display [4], [5] industries. In many cases, such short-stroke stages are connected in series with long-stroke actuators to be carried over a long range [6], [7], [8]. In such a configuration, the long-stroke stages such as robotic arms or linear motors are responsible for a rapid movement to achieve high throughput performance, while the short-stroke actuators enhance the positioning accuracy of the overall system. For the fine-position short-stroke actuators, the magnetic levitation has been one of the most popular solutions since it is capable of achieving precise fine-positioning in multiple degrees of freedom in a compact footprint [9], [10].

When such magnetically-levitated short-stroke actuators are used with high-acceleration long-stroke stages, however, it is required to withstand the high inertial force, which may lead to an excessive amount of control effort to maintain an accurate relative position with respect to the long-stroke stages. Such a requirement may introduce operation limits to the long-stroke actuators. For instance in [11], the acceleration of a robotic arm is limited to prevent the coil overheating of the serially-connected short-stroke magnetic levitator. There have been a number of studies on the Lorentz-force-type short-stroke actuators in prior art [12], [13]. Such type of actuators however show limitations in terms of the maximum force-to-mover mass ratio [14], requiring larger footprint and excessive current excitation so as to achieve the high bandwidth and compensate the high inertial force [15], [16]. Compared to Lorentz-force-type levitators, reluctance-force-type levitators achieve higher force density and therefore can be more suitable candidates for the high-throughput fine-positioning short-stroke actuators.

This paper presents the design and control methods of a novel reluctance-force-type short-stroke magnetic levitator module as a strong alternative to Lorentz-force-type magnetic levitators. The proposed levitator module is capable of fine-positioning with high bandwidths in three degrees-of-freedom (3 DOFs) to be able to withstand high inertial forces caused by serially-connected high-throughput long-stroke stages. The rest of this paper is organized as follows. Section II describes the design of the 3-DOF reluctance-force-type levitator module. Section III presents the working principle in depth, showing how the 3-DOF in-plane motions can be actively generated in a decoupled manner. Section IV discusses the experimental prototype of the levitator module and its control performance validation, and Section V concludes the paper with the discussion on how the proposed levitator module can be integrated into a 6-DOF magnetic levitation stage.

II. Design of 3-DOF Reluctance-force-type Levitator Module

A. Rotor and Stator Design

Fig. 1 shows a CAD (computer-aided design) model of the 3-DOF reluctance-force-type magnetic levitator module, which consists of a pair of stator assemblies, a single rotor assembly, and sensing systems. The U-shaped rotor assembly is composed of two iron-cores and a rotor plate. Note that the rotor plate is made of a non-magnetic material so as to isolate the magnetic flux in each side of stator-rotor assembly. The rotor is located between the two stator assemblies and is actively controlled in the three degrees-of-freedom in the XZ plane, capable of the translation motion in the X and Z directions, and a rotational motion in the θ_y direction with no mechanical contact with the stator assemblies. The other three DOFs of θ_x, θ_z, and Y are passively stabilized. The

This work was supported in part by the National Research Foundation of Korea (NRF) grant funded by the Korea government (MSIT)(No. 2020R1C1C100801313) and in part by Korea Institute for Advancement of Technology (KIAT) grant funded by the Korea government (MOTIE)(P0012744, The Competency Development Program for Industry Specialist).*(Corresponding author: Jun Young Yoon.)*

H M Yoon, J W Jung, E K Kim, J M Park, J M Sung, and J Y Yoon are with the Department of Mechanical Engineering, Yonsei University, Seoul 03722 South Korea junyoung.yoon@yonsei.ac.kr

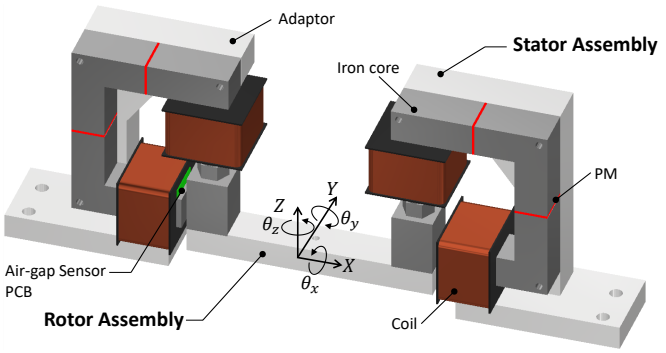

Fig. 1. CAD model of 3-DOF reluctance-force-type magnetic levitator module consisting of the rotor, stator, and sensors. The U-shaped rotor assembly is magnetically levitated and actively controlled in X, Z, and θ_y directions. The stator assembly is composed of two permanent magnets, coil windings, iron-cores (dark grey), and adaptors (light grey). A single magnetic levitator module consists of two stator assemblies and one rotor assembly. Optical-type airgap sensors are used to measure the airgap distance between the stator and the rotor.

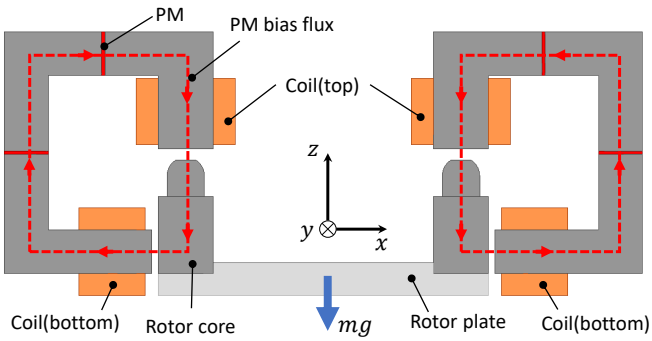

Fig. 2. Cross-sectional schematic of 3-DOF reluctance-force-type magnetic levitator module. Two PM-biased flux paths are independent to each other, but symmetrical in the YZ plane. Each biased flux links one rotor core with the corresponding stator core through two airgaps, one facing in the X-direction and the other facing in the Z-direction. Note that nominally there is no flux path between two stator assemblies. This PM-biased flux formation enables bi-directional in-plane motions in the XZ plane and also simultaneously provides the passive compensation on the rotor weight.

active control in all 6-DOFs is however possible by integrating two of these modules, which is discussed as a future work in Section V.

The stator assembly is composed of permanent magnets (PMs), iron-cores, coil windings, adaptors, and airgap-sensing modules. The PMs are located internally to the magnetic flux path to generate the biased flux, which is guided through the stator iron-cores made of a magnetic material with a high permeability. In each stator assembly, two coil windings are wound around the iron-cores to generate current-driven fluxes, and the adaptors are designed to hold iron-cores rigidly. Between the rotor and stator assemblies, there are a total of 4 airgaps. The airgap sensor modules are used to measure these airgap distances. In each sensor module, an analog optical reflective sensor (QRE1113GR from On Semiconductor) is mounted on a PCB with preset chip resistors for a desirable sensitivity and a sensing range. This sensor is widely used in applications and researches that require precise estimation of small airgaps up to a few millimeters [17], [18]. The size of the PCB airgap-sensing modules used in this magnetic levitator module prototype is 6 mm by 25 mm. To estimate displacements in the actively controlled 3-DOFs, two sensor modules are installed in each stator assembly at the iron-core faces, facing toward the rotor assembly.

B. PM-Biased Flux Distribution

The internal PMs located in the stator assembly generate the biased fluxes as shown in Fig. 2. Due to the design of the stator and the rotor iron-cores, two independent PM-biased flux paths are formed, and each path links one stator assembly with the rotor assembly as illustrated in the figure. Since the iron-cores in the rotor are rigidly connected by the rotor plate, the attraction forces between each stator iron-core and the rotor iron-core can be superposed to generate the magnetic forces and torques to the rotor assembly in the 3-DOFs with the help of the current-driven fluxes as discussed in Section IV-C.

The attraction forces at the two Z-directional airgaps generated by the PM-biased flux can passively compensate the gravitational force on the rotor assembly. The attractive forces in the other two X-directional airgaps, on the other hand, are nominally balanced out due to the symmetry of two independent PM-biased flux paths. Note that there is nominally no flux linkages between the two rotor cores and also between the two stator assemblies, as can be seen in Fig. 2. Such PM-biased flux formation ensures no magnetic interference between the levitating-force points and also on any objects that may be installed on the rotor plate.

III. Working Principle

Fig. 3 shows how the 3-DOF in-plane forces and torque are generated in the proposed magnetic levitator module. The current in each of the four coil windings is driven independently, and when the coils are excited, the current-driven flux is generated on top of the PM-biased flux, either strengthening or weakening the PM-biased flux in each of the 4 airgaps. Such controllability on the airgap fluxes leads to the control of the attractive forces between the rotor and stator iron-cores, enabling the force and torque generation in the directions of X, Z, and θ_y.

Fig. 3a shows the generation of the X-direction force F_x and the corresponding current excitation on the bottom coil windings in both stator assemblies. In order to generate a positive F_x as illustrated in Fig. 3a, the bottom coil in the right stator assembly is excited in the direction to strengthen the PM-biased flux at the right-side bottom airgap, while the bottom coil in the left stator assembly weakens the PM-biased flux. The negative F_x can be also generated by energizing the current to these coil windings in the opposite directions. Note that nominally no net Z-directional force nor θ_y-directional torque are generated by such coil excitations since the magnetic fluxes in the bottom airgaps are isolated by the magnetic design of the levitator module.

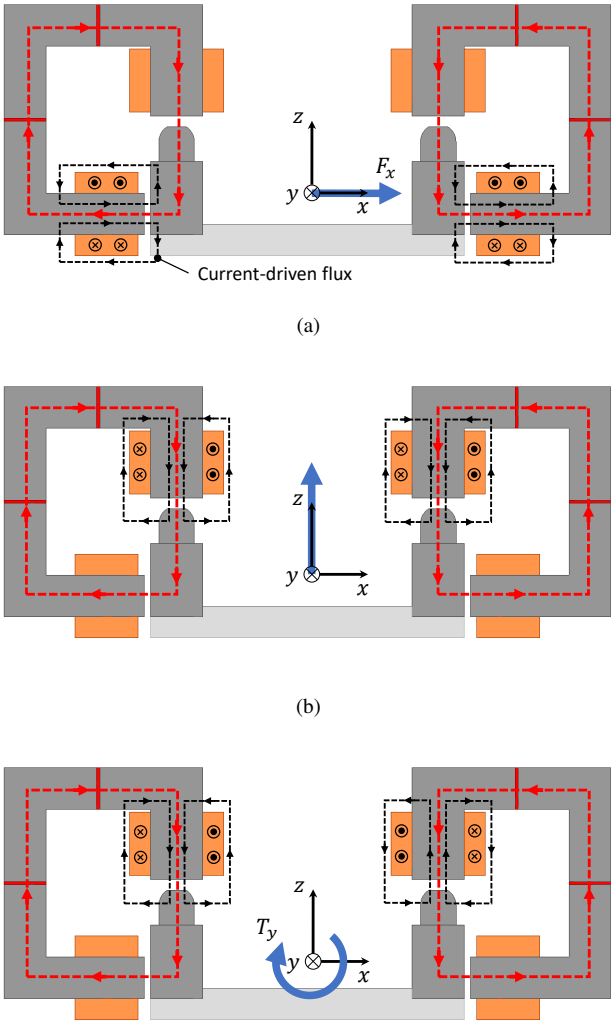

Fig. 3. Force and torque generation mechanism for the in-plane motions of the reluctance-force-type magnetic levitator module with the corresponding coil excitations. Depending on the direction of the current excitation to each coil, the current-driven flux (black dotted line) can either strengthen or weaken the PM-biased flux (red dotted line), generating (a) X-direction lateral force F_x, (b) Z-direction vertical force F_z, and (c) θ_y-direction rotational torque T_y.

Fig. 3b and Fig. 3c depicts the generation mechanism of the Z-direction force (F_z) and the θ_y-direction torque (T_y). For the Z-directional force generation, the currents at both the top coils are excited in the same direction and magnitude in a way to equally strengthen the PM-biased fluxes in the two top airgaps. The net positive F_z is then generated as shown in Fig. 3b. By exciting these top coils both in the opposite directions, the net negative F_z can be also achieved with a help of the gravitational force. As for the θ_y-direction torque generation, these two top coils are excited in the opposite direction to each other so that the Z-direction attractive force is strengthened in the one airgap while weakened in the other airgap, generating a net torque T_y as illustrated in Fig. 3c.

Since the 3-DOF force equilibriums in the XZ plane are

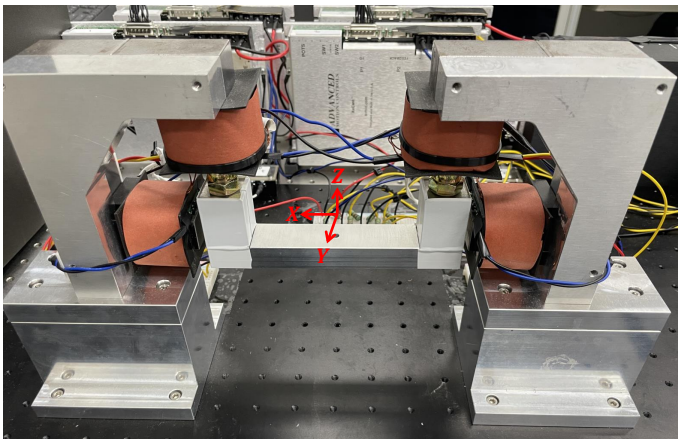

Fig. 4. Experimental testbed of 3-DOF magnetic levitator module consisting of two stator assemblies and a single rotor assembly. The nominal position of the rotor is where the lateral/bottom airgap length is 3.0 mm and the top airgap length is 4.7 mm. The coordinate frame is fixed at the center of gravity of the rotor.

TABLE I

KEY DESIGN PARAMETERS

Parameter	Value
Rotor assembly mass	0.50 kg
Stator core mass	0.96 kg
Stator coil mass	0.79 kg
Stator adaptor mass	0.55 kg
Internal PM dimension (top)	25 mm × 20 mm × 1.5 mm
Internal PM dimension (bottom)	25 mm × 25 mm × 1.5 mm
Stator assembly dimension	138 mm × 143 mm × 50 mm
Coil turns (AWG22)	473
Nominal top airgap length	4.7 mm
Nominal bottom airgap length	3.0 mm

inherently unstable due to the negative stiffnesses caused by the PM-biased fluxes, it is necessary to actively control these DOFs, especially in a decoupled manner for the precise motion control of the magnetic levitator module. Considering the aforementioned force and torque generation mechanism, the coil currents can be expressed in a matrix form of

$$\begin{pmatrix} i_1 \\ i_2 \\ i_3 \\ i_4 \end{pmatrix} = \begin{pmatrix} i_{\text{L,bottom}} \\ i_{\text{L,top}} \\ i_{\text{R,top}} \\ i_{\text{R,bottom}} \end{pmatrix} = \begin{pmatrix} -1 & 0 & 0 \\ 0 & 1 & 1 \\ 0 & 1 & -1 \\ 1 & 0 & 0 \end{pmatrix} \begin{pmatrix} u_x \\ u_z \\ u_{\theta_y} \end{pmatrix} \quad (1)$$

where u_x, u_z, and u_{θ_y} indicate control efforts in each DOF. Using the coil excitation combination, we present the control performance of the proposed magnetic levitator module in the following section.

IV. CONTROL PERFORMANCE

A. Experimental Testbed

The testbed setup for the experimental validation of the 3-DOF magnetic levitator module is shown in Fig. 4 with the key design parameters of the module prototype organized in Table. I. The total mass of one stator assembly including the

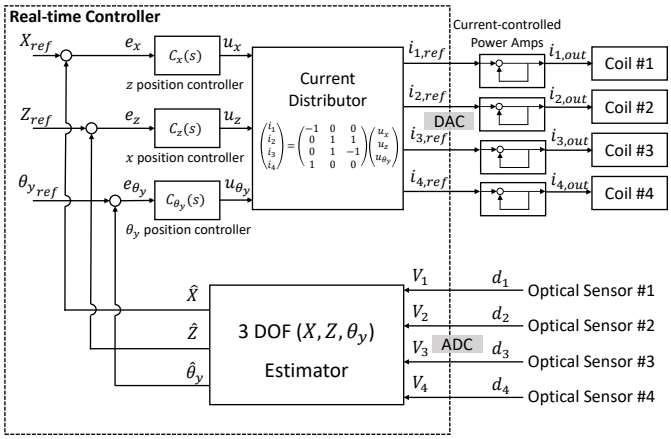

Fig. 5. Controller block diagram of 3-DOF magnetic levitator module prototype in the experimental testbed.

TABLE II
CONTROLLER PARAMETERS

DOF	K_p [A/mm]	T_i [ms]	τ [ms]	α
$C_x(s)$	2.42			
$C_z(s)$	12.01	79.58	0.23	50
$C_{\theta_y}(s)$	3.67			

stator cores, internal PMs, and stator adaptors is approximately 2.8 kg, which is considered reasonable as a payload to serially-connected long-stroke actuators. The dimension of the internal PMs (NdFeB 35) is determined so as to passively compensate the rotor mass of 0.5 kg. The four coils in the prototype are independently driven by current-controlled PWM (pulse-width modulation) power amplifiers (B30A40 by Advanced Motion Controls) to provide controlling currents required from the servo controller and to distribute the control efforts to each coil using the distribution scheme of (1). The optical reflective sensors measure the distances of airgaps with a measurement range of 1mm $\sim$ 4mm. The sensor output voltages are calibrated to estimate the translational displacements of the rotor and also the rotating displacement.

B. Controller Design

Fig. 5 shows the controller block diagram to actively control the 3-DOF in-plane displacements of the levitated rotor. The in-plane displacements of $\hat{X}$, $\hat{Z}$ and $\hat{\theta}_y$ are estimated from the measured airgap distances of d_1, d_2, d_3, and d_4 by the four optical reflective sensors. These displacement estimations are then fed back to the servo controllers to calculate the position errors of e_x, e_z, and e_{θ_y}. To minimize such errors, the three controllers of $C_x(s)$, $C_z(s)$ and $C_{\theta_y}(s)$ calculate the necessary control efforts, which are then distributed to the four current-controlled power amplifiers to drive the four coils in the prototype based on the distributing scheme of (1). Three controllers implement lead-lag compensators as

$$C(s) = K_p \cdot \frac{T_i s + 1}{T_i s} \cdot \frac{\alpha\tau s + 1}{\tau s + 1} \qquad (2)$$

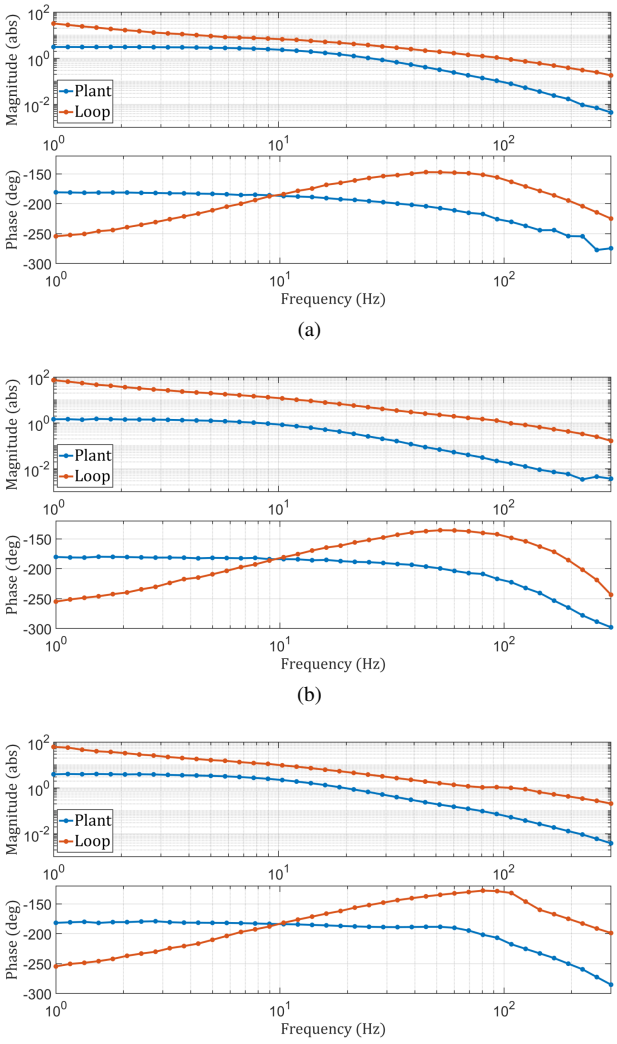

Fig. 6. Measured plant and loop frequency responses in (a) lateral X-direction, (b) levitational Z-direction, and (c) rotational θ_y-direction. The plant magnitude plots are in the unit of mm/A for the translation motions and mdeg/A for the rotational motion while the loop magnitude plots are all dimensionless.

where K_p, T_i, τ, and α indicate the proportional gain, lag compensator time constant, lead compensator time constant, and the ratio of pole to zero in the lead compensator, respectively. Table. II lists these parameters for each of the three controllers in Fig. 5. The controller parameters are determined to achieve a crossover frequency of 100 Hz in all three DOFs. The control performances of the magnetic levitator module prototype with these controllers implemented are presented in the following subsections. Note that the analog signals from the optical reflective sensors are sampled at 290 kHz in the FPGA module (NI 7846R) with a moving average of every ten samples to be used as the position feedback in a real-time controller shown in Fig. 5. The real-time controller (NI 8840) runs deterministically at 10 kHz to implement the control algorithm shown in the figure.

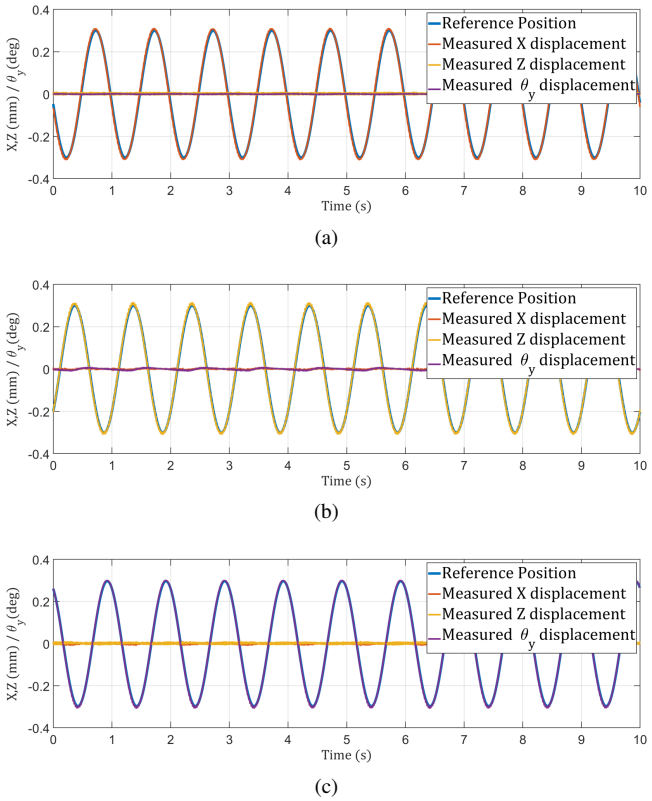

Fig. 7. Sinusoidal trajectory tracking performance in (a) X-direction, (b) Z-direction, and (c) θ_y-direction. A sinusoidal trajectory is commanded with 300 μm amplitude at 1 Hz frequency in X and Z translation. For θ_y rotation, it is commanded with 300 mdeg amplitude at 1 Hz frequency.

TABLE III

POSITION TRACKING PERFORMANCE AND COUPLED ERROR

Motion	Tracking error (RMS) X,Z (μm) / θ_y (mdeg)	Coupled error (RMS) X (μm)	Z (μm)	θ_y (mdeg)
X	12.40	-	4.30	2.16
Z	8.56	3.41	-	5.97
Y	6.56	3.41	4.25	-

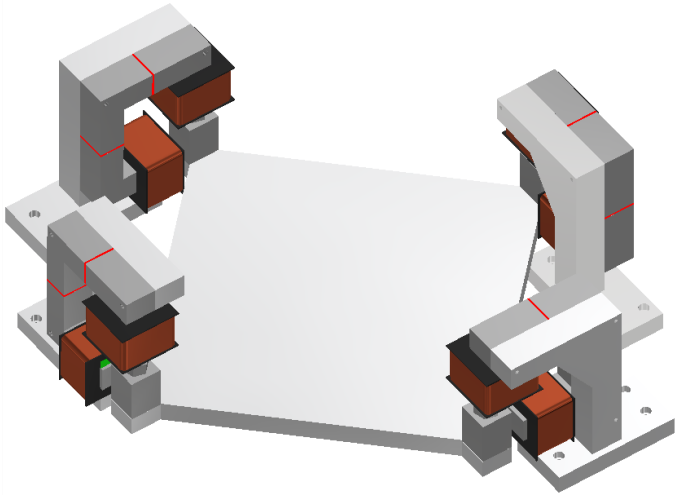

Fig. 8. Schematic CAD model of 6-DOF magnetically levitated short-stroke stage using the proposed magnetic levitator modules. Four stator assemblies are integrated with four rotor iron-cores located at the corners of the rotor stage. Note that the rotor stage structure can be freely modified depending on the applications since there is no magnetic flux penetration through the stage plate.

C. 3-DOF Levitation Control Performance

The frequency responses of the magnetic levitator module is measured in all the 3 DOFs in order to validate the control performance of the magnetic levitator module. Fig. 6 shows the measured frequency responses in the X-, Z- and θ_y-directions at the nominal position. All three measured plant frequency responses show the behavior of a system with a negative stiffness, starting the phase at -180°, which is caused by the PM-biased flux as discussed in Section III. As designed, the measured loop frequency responses show a crossover frequency of 100 Hz for all 3-DOFs. Such high crossover frequency values are sufficient to compensate for the high inertial forces that might be caused by serially-connected long-stroke actuators. In addition, we also achieve a phase margin of 20° in the X-direction, 35° in the Z-direction, and 50° in the θ_y-direction, providing proper closed-loop damping to all 3-DOFs.

D. Decoupled Control Performance

Fig. 7 shows the tracking performance of the 3-DOF reluctance-force-type magnetic levitator module in all 3-DOFs. The commanded sinusoidal trajectories have an amplitude of 300 μm for the translation motions and 300 mdeg for the rotational motion at a frequency of 1 Hz for all cases. The tracking errors and the coupled errors are organized in Table III. Note that the RMS coupled errors are as small as the sensor noise, manifesting the decoupled performance of the proposed 3-DOF levitator module.

V. CONCLUSION

In this paper, the design of the reluctance-force-type magnetic levitator module for the short-stroke stage is presented and its control performances are experimentally validated. The levitator module prototype successfully demonstrates the 3-DOF active control for the in-plane motions with the crossover of 100 Hz and the sufficient phase margin for all 3-DOFs. The decoupled control performance is also experimentally validated, showing the decoupled error is as small as the sensor noise level. We envision that the proposed levitator module can also be integrated to form a 6-DOF short-stroke stage as shown in Fig. 8. A total of four stator assemblies can be used to actively control all 6-DOFs with each pair of the stator and rotor iron-cores capable of independent control of reluctance forces in the lateral and vertical directions. We are currently working as a future research on the design and fabrication of the 6-DOF levitator for a specific application where such a 6-DOF magnetically-levitated short-stroke actuator is serially connected to high-acceleration long-stroke stages.

REFERENCES

[1] Y. Shimizu, Y. Peng, J. Kaneko, T. Azuma, S. Ito, W. Gao, and T.-F. Lu, "Design and construction of the motion mechanism of an xy micro-stage

for precision positioning," *Sensors and Actuators A: Physical*, vol. 201, pp. 395–406, 2013.

[2] D. Lee, K. Kim, K. Lee, H. Choi, N. Park, Y. Park, and M. Lee, "Robust design of a novel three-axis fine stage for precision positioning in lithography," *Proceedings of the Institution of Mechanical Engineers, Part C: Journal of Mechanical Engineering Science*, vol. 224, no. 4, pp. 877–888, 2010.

[3] H. Zhu, C. K. Pang, and T. J. Teo, "Analysis and control of a 6 dof maglev positioning system with characteristics of end-effects and eddy current damping," *Mechatronics*, vol. 47, pp. 183–194, 2017.

[4] W. Ohnishi, H. Fujimoto, K. Sakata, K. Suzuki, and K. Saiki, "Decoupling control method for high-precision stages using multiple actuators considering the misalignment among the actuation point, center of gravity, and center of rotation," *IEEJ Journal of Industry Applications*, vol. 5, no. 2, pp. 141–147, 2016.

[5] C. Young-Man *et al.*, "Design and control of a nanoprecision xy scanner," *Review of Scientific Instruments*, vol. 79, no. 4, pp. 045 109–045 101, 2008.

[6] Y.-M. Choi and D.-G. Gweon, "A high-precision dual-servo stage using halbach linear active magnetic bearings," *IEEE/ASME Transactions on Mechatronics*, vol. 16, no. 5, pp. 925–931, 2010.

[7] Q. Liu, P. Ma, S. Hu, L. Li, J. Zhu, and Z. Sheng, "Study on control strategy for coarse/fine dual-stage of step and scan lithography," in *6th International Symposium on Advanced Optical Manufacturing and Testing Technologies: Design, Manufacturing, and Testing of Smart Structures, Micro-and Nano-Optical Devices, and Systems*, vol. 8418. SPIE, 2012, pp. 210–215.

[8] H. Zhu, C. K. Pang, and T. J. Teo, "Integrated servo-mechanical design of a fine stage for a coarse/fine dual-stage positioning system," *IEEE/ASME Transactions on Mechatronics*, vol. 21, no. 1, pp. 329–338, 2015.

[9] W.-j. Kim and D. L. Trumper, "High-precision magnetic levitation stage for photolithography," *Precision engineering*, vol. 22, no. 2, pp. 66–77, 1998.

[10] Y.-M. Choi, M. G. Lee, D.-G. Gweon, and J. Jeong, "A new magnetic bearing using halbach magnet arrays for a magnetic levitation stage," *Review of scientific instruments*, vol. 80, no. 4, p. 045106, 2009.

[11] Y. Kuruma, A. Yamamoto, and T. Higuchi, "High speed non-contact object handling using magnetic levitation and tilt control," in *Applied Mechanics and Materials*, vol. 162. Trans Tech Publ, 2012, pp. 471–476.

[12] D. Wertjanz, E. Csencsics, J. Schlarp, and G. Schitter, "Design and control of a maglev platform for positioning in arbitrary orientations," in *2020 IEEE/ASME International Conference on Advanced Intelligent Mechatronics (AIM)*. IEEE, 2020, pp. 1935–1942.

[13] H. Zhang and B. Kou, "Design and optimization of a lorentz-force-driven planar motor," *Applied Sciences*, vol. 7, no. 1, p. 7, 2016.

[14] D. B. Hiemstra, G. Parmar, and S. Awtar, "Performance tradeoffs posed by moving magnet actuators in flexure-based nanopositioning," *IEEE/ASME Transactions on Mechatronics*, vol. 19, no. 1, pp. 201–212, 2012.

[15] M. Kim, J.-h. Jeong, H. Kim, and D. Gweon, "A six-degree-of-freedom magnetic levitation fine stage for a high-precision and high-acceleration dual-servo stage," *Smart Materials and Structures*, vol. 24, no. 10, p. 105022, 2015.

[16] J.-Y. Kim and D. Ahn, "Analysis of high force voice coil motors for magnetic levitation," in *Actuators*, vol. 9, no. 4. MDPI, 2020, p. 133.

[17] M. Noh, "Homopolar bearingless slice motors with magnet-free rotors for extracorporeal life support," Ph.D. dissertation, Massachusetts Institute of Technology, 2018.

[18] T. T. Hamer, "A permanent magnetic dipole reaction sphere actuator for spacecraft attitude control," Ph.D. dissertation, Massachusetts Institute of Technology, 2021.